Nonuniversal weak antilocalization effect in cubic topological Kondo insulators

Maxim Dzero, Maxim G. Vavilov, Kostyantyn Kechedzhi, and Victor M. Galitski

Phys. Rev. B **92**, 165415 — Published 14 October 2015

DOI: 10.1103/PhysRevB.92.165415

Non-universal weak antilocalization effect in cubic topological Kondo insulators

Maxim Dzero[1,2], Maxim G. Vavilov[3], Kostyantyn Kechedzhi[4] and Victor M. Galitski[5,6]
[1]*Department of Physics, Kent State University, Kent, OH 44242, USA*
[2]*Max Planck Institute for Physics of Complex Systems, Nöthnitzer str. 38, 01187 Dresden, Germany*
[3]*Department of Physics, University of Wisconsin, Madison, Wisconsin 53706, USA*
[4]*QuAIL and USRA, NASA Ames Research Center, Mail Stop 269-3, Moffett Field, CA 94035, USA*
[5]*Joint Quantum Institute and Condensed Matter Theory Center, Department of Physics, University of Maryland, College Park, Maryland 20742, USA and*
[6]*School of Physics, Monash University, Melbourne, Victoria 3800, Australia*
(Dated: September 22, 2015)

We study the quantum correction to conductivity on the surface of cubic topological Kondo insulators with multiple Dirac bands. We consider the model of time-reversal invariant disorder which induces the scattering of the electrons within the Dirac bands as well as between the bands. When only intraband scattering is present we find three long-range diffusion modes leading to weak antilocalization correction to conductivity which remains independent of the microscopic details such as Fermi velocities and relaxation times. Interband scattering gaps out two diffusion modes leaving only one long-range mode. We find that depending on the value of the phase coherence time, either three or only one long-range diffusion modes contribute to weak localization correction rendering the quantum correction to conductivity non-universal. We provide an interpretation for the results of the recent transport experiments on samarium hexaboride where weak antilocalization has been observed.

PACS numbers: 72.15.Qm, 73.23.-b, 73.63.Kv, 75.20.Hr

I. INTRODUCTION

Samarium hexaboride (SmB_6) along with PuB_6 and YbB_6 have recently emerged as prominent candidates[1–6] for hosting topologically protected metallic surface states.[7] In particular, SmB_6 - a material in which strong hybridization between samarium conduction d-electrons and strongly correlated f-electrons drives an onset of an insulating state at low temperatures[8–12] - has recently came into focus of theoretical and experimental studies as a most prominent candidate for the first correlated topological insulator.[13–23]

In order to experimentally establish the existence of the helical conduction time-reversal invariant states on a surface of a generic topological insulator using either transport or thermodynamic measurements, one needs to show that (i) the conduction at low temperatures is limited to the surface and (ii) single particle states have linear momentum dispersion along the surface and no dispersion in the normal to the surface direction and (iii) there is a strong spin-orbit interaction, which leads to coupling between the momentum and spin of the conduction electron giving rise to the helicity of the carriers. In samarium hexaboride, a series of state-of-the-art transport studies have unambiguously shown that the resistivity plateau at temperatures below 5 Kelvin[8,9] is governed by surface conduction only.[13,14,18] To verify that the conduction electrons on the surface have Dirac dispersion, G. Li et al.[16] have experimentally studied the quantum oscillations of magnetization under applied external magnetic field. By plotting the dependence of the index n which labelled the positions of the maxima in magnetization versus the inverse of magnetic field, G. Li et al. have shown that there is a contribution corresponding to the zero energy state which would only be possible for conducting state with Dirac-like dispersion. Lastly, Kim, Xia and Fisk[18] have examined the low-temperature transport properties of the alloys $Sm_{1-x}A_xB_6$ for the non-magnetic yttrium and ytterbium (A=Y,Yb) and magnetic gadolinium (A=Gd) substitutions. They found that while small amount ($\sim 3\%$) of gadolinium leads to insulating behavior in resistivity, substitutions of non-magnetic ions do not cause destruction of the metallic surface states.[18] These results indicate that magnetic impurities cause the saturation of the phase coherence time τ_ϕ, which in turn, leads to the vanishing of the quantum interference effects in transport at very low temperatures.

The magnitude of the spin-orbit interaction for the surface electrons in topological insulators can be indirectly probed by studying the quantum interference correction to conductivity:[24–28] upon decrease in temperature, $\delta T < 0$, increase in conductivity ($\delta\sigma > 0$) would signal weak anti-localization effect as opposed to weak localization corresponding to decrease in conductivity ($\delta\sigma < 0$). The sign of the correction to conductivity is determined by the ratio of the spin-orbit scattering length, l_{SO}, to the dephasing length l_ϕ: for weak spin-orbit coupling, $l_{SO} \gg l_\phi$ (here l is a mean-free path) correction to conductivity is negative, while in the opposite limit of strong spin-orbit coupling $l_{SO} \ll l_\phi$ and the interference correction to conductivity is positive.

Thus, helicity of the Dirac-like carriers on the surface of topological insulators, associated with the fixed polarization of electron spin perpendicular to the momentum direction (i.e. $l_{SO} \sim l$, here l is a mean-free path), necessarily leads to weak-antilocalization due additional Berry

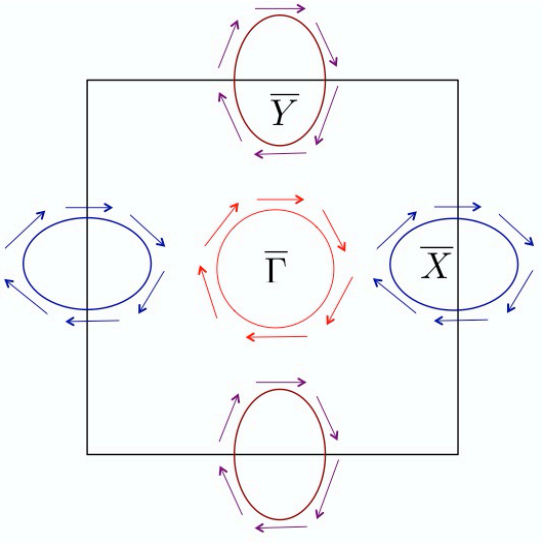

FIG. 1: (Color online) Surface band structure for the strong topological insulator emerging from the inversion of the odd and even parity bands at the X points of the bulk Brillouin zone. Arrows denote the spin texture of the surface carriers corresponding to the ground state configuration with the Γ_8 quartet of the f-levels.[19,21] We assume that chemical potential crosses all three bands. Without loss of generality we consider the bands with the same chirality. In addition we will neglect the ellipticity of the Dirac pockets, but take into account the difference in the Fermi velocities of the electrons in different pockets.

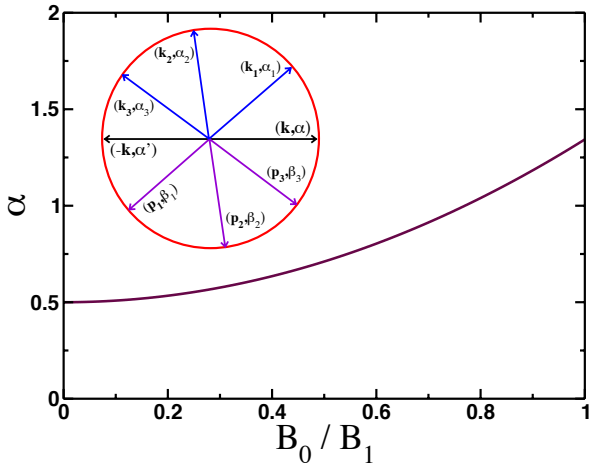

FIG. 2: (Color online) Schematic plot for the crossover behavior of the dimensionless coefficient α, appearing in Hikami-Larkin-Nagaoka expression (1.1), as a function of the ratio B_0/B_1 Eq. (4.24) for the quantum correction to conductivity for the surface states in topological Kondo insulators. The value of the remaining parameter is chosen as $B_2 = 0.9B_1$. Within the three-band model for the topological surface states, in the absence of the interband scattering there are three diffusion modes, which govern the quantum correction to conductivity with $\alpha \sim 3/2$. However, in the presence of the interband scattering processes two out of three diffusion modes become gapped, so that $\alpha \sim 1/2$. However, at moderately high temperatures when τ_ϕ becomes comparable to the gap of the remaining two diffusion modes also contribute leading to $\alpha \sim 3/2$. Inset shows two independent scattering processes from state with momentum $\mathbf{k}$ in band α to a state with momentum $-\mathbf{k}$ in band α' leading to the quantum correction to conductivity.

phase acquired by the carriers as they scatter along the time-reversed paths.[25,29]

Application of an external magnetic field perpendicular to conducting surface destroys quantum interference processes leading to positive or negative magneto-conductivity – another signature of weak localization or weak anti-localization. The corresponding magnetic field dependence of the conductivity correction is then described by famous Hikami-Larkin-Nagaoka (HLN) formula:[24]

$$\Delta\sigma_{\rm HLN}(B) = \frac{\alpha e^2}{2\pi^2\hbar}\left[\log\frac{B_0}{B} - \psi\left(\frac{1}{2}+\frac{B_0}{B}\right)\right], \quad (1.1)$$

where α is a dimensionless parameter determined by the number of conduction channels and the strength of the spin-orbit coupling, ψ is the digamma function, $B_0 = \hbar/4el_\phi^2$. Moreover, $\alpha > 0$ for the case of the strong spin-orbit coupling and each independent conduction channel contributes $1/2$ to the value of α, so that $\alpha = 1$ for the case of Rashba-split bands on the surface. For the topological surface states, $\alpha = 1/2$ for the case of a single Dirac band and $\alpha = 3/2$ for the three Dirac bands.

Recently, S. Thomas et al.[30] have studied weak anti-localization effect and magneto-conductivity in samarium hexaboride. By fitting the experimental data with HLN formula, Eq. (1.1) for the case of a single band, the value of the parameter α came out to be approximately equal to one, $\alpha \approx 1$, for several sets of data. In the most recent transport experiments by Y. Nakajima et al.[31] also observe weak-antilocalization effect and their results seem to be generally in agreement with the earlier studies. On the other hand, these observations would contradict a natural expectation that the value of alpha must be close to $\alpha \approx 3/2$, which is due to the three Dirac bands on the surface of SmB_6.[2,5,32,33].

Motivated by these experimental results, we calculate the quantum interference correction to conductivity in a generic cubic topological Kondo insulator. Our main goal is to account for the fairly wide distribution of values for the parameter α obtained by analyzing the experimental data.[30,31]. As we argue in this paper, the presence of the disorder-induced interband scattering suppresses two antilocalization modes and reduces the value of α from naive $\alpha = [1/2 \times \text{number of zones}]$. We consider the surface band structure which consists of three Fermi pockets: one at surface $\overline{\Gamma}$ point and two at $\overline{X}$ and $\overline{Y}$ points of the two-dimensional Brillouin zone, Fig. 1. We assume that the electron scattering within each band - intraband scattering - provides the strongest scattering mechanism, so that elastic scattering time is the shortest

time scale in the problem. Consequently, the disorder scattering between various bands is considered as a correction to the intraband one. We show that (i) for the case when only intraband disorder time-reversal invariant scattering is present, all three conduction channels (per surface) will contribute to the interference correction to conductivity; (ii) the inclusion of the interband scattering shows that two conduction channels are suppressed while the remaining one contributes to weak anti-localization effect. However, at higher temperatures when the inverse dephasing time $\tau_\phi^{-1} \sim T^p$ $(p > 0)$ becomes comparable with the size of the gap in the spectrum of the diffusion modes, we still find that all three modes contribute to conductivity. By considering τ_ϕ as a parameter, we describe this crossover behavior by showing the dependence of the parameter α on τ_ϕ schematically on Fig. 2. For the analysis of magnetoconductivity using HLN formula (1.1) our result implies that the size of the correction for small fields and the large fields generally would correspond to different values of α. Specifically, we will show that the (1.1) generalizes to

$$\Delta\sigma(B) = \frac{e^2}{2\pi^2\hbar}\sum_{i=0}^{2}\alpha_i\left[\log\frac{B_i}{B} - \psi\left(\frac{1}{2}+\frac{B_i}{B}\right)\right], \quad (1.2)$$

where α_i are the dimensionless parameters, which depend on the diffusion coefficients of the surface electrons from each band and scattering times and $B_{1,2}$ are determined by the interband scattering times, which give rise to the gap in the long-range diffusion modes, while $B_{i=0} = \hbar/4el_\phi^2$ is still defined by the inelastic dephasing length l_ϕ.

Furthermore, we find that in the prefactor α can be expressed in terms of the diffusion coefficient for each Dirac band and scattering times as follows:

$$\alpha = \sum_a w_{0a}\frac{D_a}{2D}\left(2 - \frac{\tau_a}{\tau_{a0}}\right)\frac{\tau_t}{\tau_{a0}}, \quad (1.3)$$

where D_a $(a = \Gamma, X, Y)$ are the diffusion coefficients for each Dirac band, τ_a, τ_{a0} are the scattering times in the presence or absence of the interband scattering correspondingly, $\tau_t^{-1} = \tau_\Gamma^{-1} + \tau_X^{-1} + \tau_Y^{-1}$ and w_{0a} are the dimensionless weight factors. Diffusion coefficient D in (1.3) in (1.3) is determined by the combination of D_a and τ_a (see e.g. Eq. (4.18)). Therefore, depending on the temperature at which the experiments are performed and on the surface disorder one, expects that the values of the parameter α extracted by fitting the experimental data using (1.1) and (1.2) may vary from $\alpha \sim 1/2$ to $\alpha \sim 3/2$ for the case of three Dirac bands. This situation is schematically shown on Fig. 2.

More importantly, even in the limit of zero temperatures the value of the parameter α remains non-universal. Indeed, if we consider Eq. (1.3) and take the limit of the infinitely large interband scattering times, it follows $\tau_a \to \tau_{a0}$, $w_{0a} \to 1$ and, as a result $\alpha \to 3/2$. However, for the finite interband scattering rates, $\alpha = 1/2$ provides a lowest bound for the possible values of α.

Our paper is organized as follows. In Section II we introduce the model for the surface states. In Section III we present the calculation of the interference correction to conductivity for the uncorrelated mixture of the intraband and interband disorder potentials. In Section IV we generalize the results from the previous Sections to the case of the correlated mixture of the scattering potentials. Sections V and VI are devoted to the discussion of our results and conclusions. Throughout the paper we adopt the energy units $\hbar = c = 1$.

II. SURFACE STATES IN THE PRESENCE OF DISORDER

In this Section we setup the model and introduce the parameters which will be used in the calculation for the interference correction to conductivity.

A. Hamiltonian and correlation functions

The Hamiltonian for the surface electrons in cubic topological Kondo insulators can be written as a sum of three terms, which describe electrons near $\overline{\Gamma}$, $\overline{X}$ and $\overline{Y}$ points in the 2D Brillouin zone, Fig. 1:[2,5,32,33]

$$\hat{H} = \sum_{j=\Gamma,X,Y}\sum_{\mathbf{p}\sigma}\psi^\dagger_{j\mathbf{p}\sigma}v_j(\vec{\sigma}\cdot\vec{p})\psi_{j\mathbf{p}\sigma}. \quad (2.1)$$

Here we neglect the anisotropies in velocities along x and y-direction in $\overline{X}$ and $\overline{Y}$ pockets.[2,33] In Eq. (2.1) momentum is taken relative to the center of the pocket. Introducing the six component spinor

$$\hat{\Psi}^T = [\psi_{\Gamma\mathbf{p}\uparrow}\ \psi_{\Gamma\mathbf{p}\downarrow}\ \psi_{X\mathbf{p}\uparrow}\ \psi_{X\mathbf{p}\downarrow}\ \psi_{Y\mathbf{p}\uparrow}\ \psi_{Y\mathbf{p}\downarrow}] \quad (2.2)$$

the Hamiltonian can be compactly written as follows

$$\hat{H} = v\vec{\Sigma}\cdot\vec{p}, \quad \vec{\Sigma} = \Pi_v\otimes\vec{\sigma}, \quad \Pi_v = \begin{pmatrix}\zeta_\Gamma & 0 & 0\\ 0 & \zeta_X & 0\\ 0 & 0 & \zeta_Y\end{pmatrix} \quad (2.3)$$

and the coefficients $\zeta_{\Gamma,X,Y} = v_{\Gamma,X,Y}/v$ account for velocity anisotropies on different pockets. The underlying cubic symmetry requires $v_X = v_Y$, however there is no symmetry constrains on the ratio of velocities at Γ and X, Y pockets, so that generally $v_\Gamma \neq v_{X,Y}$. In addition, we define the retarded and advanced Green's functions:

$$\check{G}_0^{R,A}(\mathbf{p},\epsilon) = \begin{bmatrix}\hat{G}_{0\Gamma}^{R,A}(\mathbf{p},\epsilon) & & 0\\ & \hat{G}_{0X}^{R,A}(\mathbf{p},\epsilon) & \\ 0 & & \hat{G}_{0Y}^{R,A}(\mathbf{p},\epsilon)\end{bmatrix},$$
$$\hat{G}_{0j}^{R,A}(\mathbf{p},\epsilon) = \frac{(\epsilon\pm i\delta)\hat{\sigma}_0 + v_j(\vec{\sigma}\cdot\vec{p})}{(\epsilon\pm i\delta)^2 - v_j^2p^2}. \quad (2.4)$$

Note that in the Hamiltonian (2.3) we ignore the higher order terms in momentum as well as other type of conduction channels which may arise due to polarity driven

bands,[34] strong surface potential[33] etc. We will discuss how the presence of additional terms in the Hamiltonian may affect our results in Section V.

B. Intraband disorder

In the following we construct a theory of the metallic conductance of the disordered surface state of SmB_6 using perturbative expansion in $p_F l \gg 1$. The values estimated from experiments $p_F l \sim 100$ suggest the perturbation theory to be a good approximation for the data[23]. We consider N_i impurities with potential u_0 and matrix structure described by $\hat{U}$ leading to the following expression

$$\hat{V}(\mathbf{r}) = u_0 \hat{U} \sum_i \delta(\mathbf{r} - \mathbf{R}_i). \tag{2.5}$$

Averaging over an impurity ensemble yields

$$\begin{aligned} &\hat{V}(\mathbf{p}) = \sum_i u_0 \hat{U} e^{i\mathbf{p}\cdot\mathbf{R}_i}, \quad \langle \hat{V}(\mathbf{p}) \rangle_{dis} = 0, \\ &\langle \hat{V}(\mathbf{p}_1)\hat{V}(\mathbf{p}_2)\rangle_{dis} = n_i \mathcal{A} u_0^2 \hat{U}\hat{U}\delta(\mathbf{p}_1 + \mathbf{p}_2), \end{aligned} \tag{2.6}$$

where $\mathcal{A}$ is the surface area and $n_i = N_i/\mathcal{A}$. In the following we first consider the intraband disorder, which implies that matrix $\hat{U}$ has the following block-diagonal structure:

$$\hat{U} = \hat{I}_{3\times 3} \otimes \hat{\sigma}_0, \tag{2.7}$$

where $\hat{I}_{3\times 3}$ is a unit matrix. We first evaluate the disorder averaged correction to the self-energy:

$$\check{\Sigma}(\epsilon) = n_i u_0^2 \int \frac{d^2\mathbf{p}}{(2\pi)^2} \hat{U} \check{G}_0^{R,A}(\mathbf{p}, \epsilon) \hat{U} \tag{2.8}$$

Clearly, $\check{\Sigma}(\epsilon)$ has a block-diagonal matrix structure similar to the expression for the retarded and advanced propagators (2.4). It follows

$$\hat{\Sigma}_j(\epsilon) \approx \mp \frac{i\hat{\sigma}_0}{2\tau_{j0}}, \quad \tau_{j0}^{-1} = \pi n_i \nu_j u_0^2. \tag{2.9}$$

where τ_{j0} is elastic scattering rate, we neglected the real part since it leads to a small correction to $\epsilon \approx v_j p_{Fj}$, p_{Fj} are the corresponding Fermi momenta and ν_j is a single particle density of states per spin $\nu_j = p_{Fj}/2\pi v_j$. The corresponding expressions for the renormalized retarded and advanced correlators become

$$\hat{G}_j^{R,A}(\mathbf{p}, \epsilon) = \frac{(\epsilon \pm i/2\tau_{j0})\hat{\sigma}_0 + v_j(\vec{\sigma}\cdot\vec{p})}{(\epsilon \pm i/2\tau_{j0})^2 - v_j^2 p^2}. \tag{2.10}$$

Similar expression for the correlation functions has been found for graphene.[35]

C. Classical conductivity

Next, we can use the expressions for the correlators (2.10) to calculate the classical conductivity, which is given by

$$\sigma_{\alpha\beta}(\omega) = \frac{e^2}{2\pi} \int \frac{d^2\mathbf{p}}{(2\pi)^2} \mathrm{Tr}\left\{ \hat{v}_\alpha \check{G}^R(\mathbf{p}, \epsilon+\omega) \hat{v}_\beta \check{G}^A(\mathbf{p}, \epsilon) \right\}. \tag{2.11}$$

Here $\hat{v}_\alpha$ are the components of the velocity defined by the momentum derivative of the Hamiltonian (2.3) $\hat{v}_\alpha = \vec{\nabla}_{p_\alpha} \hat{H} = v\hat{\Sigma}_\alpha$. The block-diagonal structure of matrices entering into (2.11) allows one to write

$$\sigma_{\alpha\beta}^{(0)}(\omega) \approx \delta_{\alpha\beta} \sum_j \frac{e^2 \nu_j v_j^2 \tau_{j0}}{2(1 - i\omega\tau_{j0})} \tag{2.12}$$

where the subscript denotes that we have neglected the vertex corrections and on the last step we have assumed $\epsilon \gg \{\omega, \tau_{j0}^{-1}\}$. The vertex corrections can be formally included by making the following substitution in (2.11):

$$\hat{v}_\alpha \to \Lambda \int \frac{d^2\mathbf{p}}{(2\pi)^2} \hat{U} \check{G}^A(\epsilon, \mathbf{p}) \hat{v}_\alpha \check{G}^R(\epsilon+\omega, \mathbf{p}) \hat{U} \tag{2.13}$$

Summing the resulting geometric series to all orders we obtain

$$\sigma_{\alpha\beta}(\omega) = \sum_j \frac{e^2 \nu_j v_j^2 \tau_{\mathrm{tr},j}}{2(1 - i\omega\tau_{\mathrm{tr},j})}, \quad \tau_{\mathrm{tr},j} = 2\tau_{j0}. \tag{2.14}$$

Thus, we find for the Dirac electrons the transport lifetime for the conducting states is twice the elastic scattering time.[35]

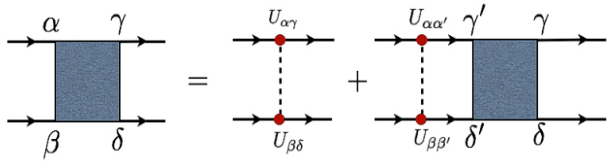

FIG. 3: (Color online) Dyson equation for the Cooperon propagator $\Gamma_{\alpha\beta,\gamma\delta}(\omega, \mathbf{q})$. Here the Greek indices encode both spin and Dirac cone - "valley" - components, solid lines represent the single particle propagators and $\hat{U}$ accounts for the disorder potential.

D. Cooperon Propagator

The quantum interference correction to conductivity (2.14) is associated with the two-particle correlation function known as the Cooperon. It satisfies the Bethe-Salpeter equation which is represented diagrammatically on Fig. 3. In what follows, we will use separate notations for the "valley" and "spin" indices: we adopt latin superscripts for valley $a = 1, 2, 3$ and Greek subscripts

for components of the Kramers doublet. Equation for the Cooperon propagator reads:

$$\Gamma^{ab,cd}_{\alpha\beta,\gamma\delta}(\omega,\mathbf{q}) = \Lambda_0 U^{ac}_{\alpha\gamma}U^{bd}_{\beta\delta} + \Lambda_0\sum\int\frac{d^2\mathbf{p}}{4\pi^2}U^{aa'}_{\alpha\alpha'}[\check{G}^R]^{a'c'}_{\alpha'\gamma'}(\epsilon+\omega,\mathbf{p}) \times\Gamma^{c'd',cd}_{\gamma'\delta',\gamma\delta}(\omega,\mathbf{q})U^{bb'}_{\beta\beta'}[\check{G}^A]^{b'd'}_{\beta'\delta'}(\epsilon,\mathbf{q}-\mathbf{p}), \tag{2.15}$$

with $\Lambda_0 = n_i u_0^2$ and the summation goes over repeated indices. Since $\check{G}^{A,R}_{\alpha\beta}$ are diagonal in "valley" indices, we have

$$[\check{G}^{A,R}]^{ab}_{\alpha\beta}(\epsilon,\mathbf{p}) = [\hat{G}^{R,A}_a(\epsilon,\mathbf{p})]_{\alpha\beta}\delta_{ab} \tag{2.16}$$

Next for convenience we introduce the spin singlet and triplet components of the Cooperon[35,36] and define

$$C^{ab,cd}_{S_1S_2}(\omega,\mathbf{q}) = \frac{1}{2}\sum(\sigma_y\sigma_{S_1})_{\alpha\beta}\Gamma^{ab,cd}_{\alpha\beta,\gamma\delta}(\omega,\mathbf{q})(\sigma_{S_2}\sigma_y)_{\delta\gamma}, \tag{2.17}$$

where $S_{1,2} = 0,x,y,z$. Using the following identities

$$\sum_{S=0,x,y,z}(\sigma_S\sigma_y)_{\alpha\beta}(\sigma_y\sigma_S)_{\mu\nu} = 2\delta_{\alpha\nu}\delta_{\beta\mu}, \quad \sum_{a=x,y,z}[\sigma_a]_{\alpha\beta}[\sigma_a]_{\mu\nu} = 2\delta_{\alpha\nu}\delta_{\beta\mu} - \delta_{\alpha\beta}\delta_{\mu\nu}, \tag{2.18}$$

we can now express the components of Cooperon (2.15) in the right hand side in terms of matrices (2.17) using

$$\Gamma^{ab,cd}_{\alpha\beta,\gamma\delta}(\omega,\mathbf{q}) = \frac{1}{2}\sum_{S_1,S_2}(\sigma_{S_1}\sigma_y)_{\beta\alpha}C^{ab,cd}_{S_1S_2}(\omega,\mathbf{q})(\sigma_y\sigma_{S_2})_{\gamma\delta}, \tag{2.19}$$

which follows directly from relations (2.17) and (2.18). To obtain the equation for the singlet and triplet components of the Cooperon, we multiply both parts of the equation (2.15) by the product of Pauli matrices introduced in (2.17).

III. INTRABAND SCATTERING

A. Gapless cooperon modes

To keep our calculations transparent, in this section we analyze the system with intraband scattering only and postpone treatment of the interband scattering for the next section. Here the matrix for the intraband disorder potential is diagonal in both spin and valley indices (2.7). In the momentum integral we insert equation (2.19). This gives an overall prefactor of $(1/2)^2$ in front of the second term, but the subsequent trace over the product of Pauli matrices will cancel one of them. It follows

$$C^{ab,a'b'}_{S_1S_2}(\omega,\mathbf{q}) = \Lambda_0\delta_{aa'}\delta_{bb'}\delta_{S_1S_2} + \frac{\Lambda_0}{2}\sum\int\frac{d^2\mathbf{p}}{4\pi^2}(\sigma_y\sigma_{S_1})_{\alpha\beta}[\hat{G}^R_a(\epsilon+\omega,\mathbf{p})]_{\alpha\gamma'} \times[\hat{G}^A_b(\epsilon,\mathbf{q}-\mathbf{p})]_{\beta\delta'}(\sigma_S\sigma_y)_{\delta'\gamma'}C^{ab,a'b'}_{SS_2}(\omega,\mathbf{q}) \tag{3.1}$$

Clearly, there are two possibilities: (i) when the retarded and advanced propagators belong to the same valley, i.e. $a = b = a' = b'$ and (ii) when they belong to different bands or valleys, $a \neq a', b \neq b'$. To evaluate the trace under the integral we recall the definition of the Greens functions (2.10) which are diagonal in the band index a, b. Electric conductivity is given by a trace over band indexes in Eq. (2.11) and therefore in the absence of interband scattering only Cooperon components that are diagonal in band indexes contribute to quantum corrections to conductivity. For a diagonal Cooperon each term in Eq. (3.1) is diagonal in band indexes and therefore the system of equations splits into a set of independent equations for each band. Thus, we only need to consider the components $C^a_{S_1S_2}(\omega,\mathbf{q})$ defined in the same band, Fig. 4. After short calculation we find that the equation for the components of the Cooperon matrix in the valley $a = \Gamma, X, Y$ can be compactly written as follows:

$$\hat{M}_a\cdot\hat{C}^a = \Lambda_a\hat{I}_{4\times4}. \quad \Lambda_a = \tau_{a0}^{-1}\Lambda_0 \tag{3.2}$$

and the elements of the matrix $\hat{M}$ are given by Eq. (A9) in Appendix A. In limit of $\omega\tau_{a0} \ll 1$ and $v_aq \ll 1$ for the matrix $\hat{M}_a$ we find:

$$\hat{M}_a = \begin{bmatrix} \frac{v_a^2q^2\tau_{a0}}{2} - i\omega & -\frac{i}{2}v_aq_x & -\frac{i}{2}v_aq_y & 0 \\ -\frac{i}{2}v_aq_x & \frac{1}{2}\left(\frac{1}{\tau_{a0}} - i\omega\right) & 0 & 0 \\ -\frac{i}{2}v_aq_y & 0 & \frac{1}{2}\left(\frac{1}{\tau_{a0}} - i\omega\right) & 0 \\ 0 & 0 & 0 & \frac{1}{\tau_{a0}} \end{bmatrix}. \tag{3.3}$$

To find the components of the Cooperon matrix we need to find an inverse of the matrix $\hat{M}_a$. The quantum correction to conductivity is determined by the diagonal components C^a_{ii} of the Cooperon matrix. The singlet component is given by

$$C^a_{00}(\omega,q) = \frac{\Lambda_0}{v_a^2\tau_{a0}^2q^2 - i\omega\tau_{a0}}, \tag{3.4}$$

while for the three triplet components we get

$$C^a_{xx}(\omega,q) = \Lambda_0\frac{v_a^2q^2\tau_{a0}^2(1+\sin^2\phi_q) - 2i\omega\tau_{a0}}{v_a^2\tau_{a0}^2q^2 - i\omega\tau_{a0}}, \quad C^a_{yy}(\omega,q) = \Lambda_0\frac{v_a^2q^2\tau_{a0}^2(1+\cos^2\phi_q) - 2i\omega\tau_{a0}}{v_a^2\tau_{a0}^2q^2 - i\omega\tau_{a0}}, \quad C^a_{zz}(\omega,q) = \Lambda_0. \tag{3.5}$$

Thus we find that for the *intraband disorder* out of four Cooperon modes per each Fermi pocket, only one mode - singlet modes $C^a_{00}(\omega,q)$ - remains gapless: propagation of electrons from Fermi pockets remains uncorrelated. This is not surprising given the strong spin-orbit coupling for the surface electrons.

B. WAL correction to conductivity

As we have just demonstrated, the singlet channel is the most singular one (4.7), so that we can ignore the

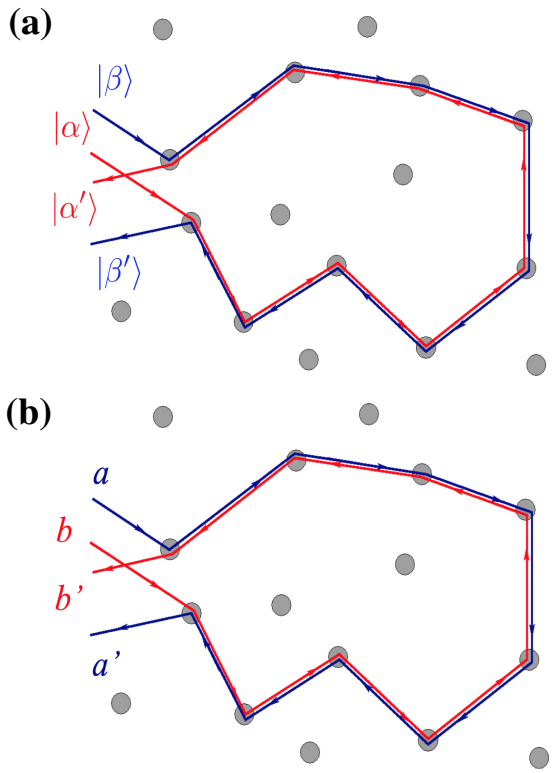

FIG. 4: (Color online) (a) Pseudospin is coupled to momentum via strong spin-orbit coupling. As a result only one mode $(|\uparrow\downarrow\rangle - |\downarrow\uparrow\rangle)/\sqrt{2}$ corresponding to a total pseudospin $S = 0$ state - singlet mode - survives; (b) Propagation of electrons from different bands is completely uncorrelated as bands have different Fermi energies and velocities (see text for details). As a result we only need to consider $a = b$ case. Even in the case of the interband scattering, the propagation of the chiral electrons still remains coherent.

correction to conductivity arising from the triplet components. Thus, for the singular weak localization correction (see Appendix B for details) we find

$$\delta\sigma(0) \approx \sum_{a=\Gamma,X,Y} e^2\nu_a v_a^2\tau_{a0}^3 \int C_{00}^a(\omega,\mathbf{q})\frac{d\mathbf{q}}{(2\pi)^2}. \quad (3.6)$$

Carrying out the momentum integral, we find

$$\delta\sigma(0) = \frac{e^2}{4\pi^2}\sum_{a=\Gamma,X,Y}\log\left(\frac{\tau_\phi}{\tau_{a0}}\right), \quad (3.7)$$

where τ_ϕ is the phase coherence time. Since $\delta\sigma(0) > 0$ the inteference correction leads to weak antilocalization. Lastly, we remind the reader that on symmetry grounds $\tau_{X0} = \tau_{Y0} \neq \tau_{\Gamma 0}$.

In an external magnetic field, the momentum integral should be replaced with the sum over Landau levels. Specifically, in the presence of the perpendicular magnetic field B, we make the standard substitution: $q_n^2 = (n + 1/2)l_B^{-2}$ with $l_B^2 = 1/4eB$. Setting $-i\omega = \tau_\phi^{-1}$ in the formula for the Cooperon and performing the summation over Landau levels yields the following expression for the magneto-conductivity $\delta\sigma(B)$:

$$\delta\sigma(B) = \frac{e^2}{2\pi^2} \times \sum_{a=\Gamma,X,Y}\frac{1}{2}\left\{\Psi\left[\frac{1}{2}+\frac{B_{0a}}{B}\left(\frac{\tau_\phi}{\tau_{a0}}\right)\right] - \Psi\left[\frac{1}{2}+\frac{B_{0a}}{B}\right]\right\}, \quad (3.8)$$

where we took into account the leading (gapless) contribution to the Cooperon, $B_{a0} = 1/4eD_a\tau_\phi$, $\Psi(z)$ is the digamma function, and we assume that τ_ϕ is the same for all bands. The first digamma function in this expression can be replaced with $\log(B_{0a}\tau_\phi/B\tau_{a0})$ due to the fact that $\tau_{a0} \ll \tau_\phi$, so that the term depending on the ratio τ_ϕ/τ_{a0} drops out of $\Delta\sigma(B) = \delta\sigma(B) - \delta\sigma(0)$. As a result, we can immediately identify the pre-factor α in Eq. (1.1) from Eq. (3.8) as $\alpha = 3/2$. This value of α is a simple consequence of the fact that for a three band model without interband scattering each band gives a universal contribution to the WAL correction to the conductivity.

IV. INTERBAND DISORDER

Now we consider the disorder potential which also includes the component which induces the scattering between the different pockets: we expect the latter to remove the divergent nature of some of the singlet Cooperon components C_{00}. Without loss of generality we will consider perhaps the simplest type of the interband disorder potential:

$$V(\vec{r}) = u_0\sum_i \hat{U}_0\delta(\vec{r}-\vec{r}_i) + u_x\sum_j \hat{U}_x\delta(\vec{r}-\vec{r}_j),$$
$$\hat{U}_0 = \hat{\tau}_0\times\hat{\sigma}_0, \quad \hat{U}_x = \hat{T}_x\times\hat{\sigma}_0. \quad (4.1)$$

Here, $\hat{T}_x$ is a 3×3 matrix whose diagonal elements all equal to zero, while off-diagonal elements equal to one: $[\hat{T}_x]_{ab} = (1-\delta_{ab})$. Just as in the case of the weak antilocalization in graphene,[35] one can show that this disorder potential captures the essential physical features needed to describe the long-range diffusion modes. Indeed, disorder potential (4.1) breaks the symmetry associated with the existence of three independent valleys and, as a consequence, we expect fewer number of the gapless diffusion modes. Moreover, we assume that any given impurity does not scatter electrons simultaneously between different pockets and within the same pocket - no correlations between the impurity scattering - so that for disorder average we have

$$\langle V(\vec{r}_1)V(\vec{r}_2)\rangle_{dis.} = \Lambda_0\hat{U}_0\hat{U}_0\delta(\vec{r}_1-\vec{r}_2) + \Lambda_x\hat{U}_x\hat{U}_x\delta(\vec{r}_1-\vec{r}_2), \quad (4.2)$$

where $\Lambda_0 = n_{i0}u_0^2$ and $\Lambda_x = n_{ix}u_x^2$ with n_{ix} being the concentration of the interband scatterers. We define the

corresponding scattering times

$$\tau_{ab}^{-1} = \pi n_{ix} u_x^2 \nu_b,\ \tau_a^{-1} = \tau_{a0}^{-1} + \sum_{b\neq a} \tau_{ab}^{-1}, \tag{4.3}$$

with the second expression following directly from Eqs. (2.8,4.1,4.2), while intraband scattering time τ_{a0} is defined by Eq. (2.9). The notations we adopt for the scattering times in (4.3) should be understood as follows: for $a, b = \Gamma, X, Y$ and the remaining scattering times are obtained by cycling permutation of these indices. Note, that our choice of the interband disoroder potential leads to $\tau_{\Gamma X} = \tau_{YX}$ but at the same time $\tau_{\Gamma X} \neq \tau_{X\Gamma}$, since the density of states at the Γ pocket is not equal to the density of states at the X pocket. The corresponding self-energy correction to the single particle Green's function at the pocket $a = \Gamma, X, Y$ (2.4) now reads

$$\hat{\Sigma}_a^{R,A}(\epsilon) \approx \mp \frac{i\hat{\sigma}_0}{2\tau_a}. \tag{4.4}$$

A. Cooperon modes in presence of interband scattering

As we have already mentioned above our goal in this section is to verify if the gapless singlet Cooperon modes acquire a gap due to interband scattering effects. In what follows we will ignore the triplet Cooperon components - they are gapped already - and obtain the equation for the singlet Cooperon components only. The corresponding equation for the pseudospin components (in the valley space) of the Cooperon matrix can be obtained similarly to Eq. (3.1). It follows:

$$\begin{aligned} &C_{00}^{ab,a'b'}(\omega,\mathbf{q}) = \Lambda_0 \delta_{aa'}\delta_{bb'} + \Lambda_x [\hat{U}_x]_{aa'}[\hat{U}_x]_{bb'} + \\ &+ \sum_{a''b''} \mathcal{M}_{aa'',bb''}(\omega,\mathbf{q}) C_{00}^{a''b'',a'b'}(\omega,\mathbf{q}), \end{aligned} \tag{4.5}$$

where we introduced the following matrix

$$\begin{aligned} &\mathcal{M}_{aa',bb'}(\omega,\mathbf{q}) = \frac{\Lambda_0}{2}\sum \int \frac{d^2\mathbf{p}}{4\pi^2} (\sigma_y)_{\alpha\beta} \\ &\times [\hat{G}_a^R(\epsilon+\omega,\mathbf{p})]_{\alpha\gamma'} [\hat{G}_b^A(\epsilon,\mathbf{q}-\mathbf{p})]_{\beta\delta'} (\sigma_y)_{\delta'\gamma'} \delta_{aa'}\delta_{bb'} + \\ &+ \frac{\Lambda_x}{2}\sum \int \frac{d^2\mathbf{p}}{4\pi^2} [\hat{U}_x]_{aa'} (\sigma_y)_{\alpha\beta} [\hat{G}_{a'}^R(\epsilon+\omega,\mathbf{p})]_{\alpha\gamma'} \\ &\times [\hat{G}_{b'}^A(\epsilon,\mathbf{q}-\mathbf{p})]_{\beta\delta'} (\sigma_y)_{\delta'\gamma'} [\hat{U}_x]_{bb'} \end{aligned} \tag{4.6}$$

for convenience and summations are performed over repeated spin and pseudospin indices.

In presence of inter-band scattering it is important to take into account the off-diagonal elements of the Cooperons in the band space, i.e. consider the full 9×9 matrix (with spin indexes $S = S_1 = 0$). This consideration is significantly simplified due to the effect of the Fermi line missmatch between different bands, due to Γ and X, Y bands having different Fermi velocities. Furthermore, X and Y bands are characterized by asymmetric Fermi lines, see Fig. 1. The resulting missmatch of the phases of wave functions results in: (i) suppression of the disorder induced interband scattering matrix element due to the Fermi wavelength missmatch; (ii) suppression of the contribution of the interband terms to the conductivity $\propto 1/((p_a - p_b)l)$, where p_a, p_b are Fermi momenta for bands a and b; (iii) suppression of the interband interference Cooperon modes with $a \neq b$ or $c \neq d$ in Eq. (4.5) due to Fermi line assymetry. The latter effect is somewhat analogous to the Fermi line trigonal warping effect in the band structure of graphene[35] and is present even in the case of very small Fermi line missmatch with an important distinction that in SmB_6 considered here it suppresses interband interference. In SmB_6 it is likely that $(p_a - p_b)l \gg 1$ for all bands and therefore the mechanism (ii) is significant. Formally this means that in the case of interband terms in the Cooperon and Hikami boxes calculated in Appendix A and C would be smaller by factor of $1/((p_a - p_b)l$ as compared to the ones corresponding to intraband terms. Therefore, we only need to consider nine elements in the Cooperon matrix: three diagonal ones $C_{00}^{aa,aa} \equiv C_{00}^{a}$ and six off-diagonal ones: $C_{00}^{aa,bb} \equiv C_{00}^{ab}$. Consequently, we introduce the following notations:

$$\hat{C} \approx \begin{pmatrix} C_{00}^{\Gamma} & C_{00}^{\Gamma X} & C_{00}^{\Gamma Y} \\ C_{00}^{X\Gamma} & C_{00}^{X} & C_{00}^{XY} \\ C_{00}^{Y\Gamma} & C_{00}^{YX} & C_{00}^{Y} \end{pmatrix} \tag{4.7}$$

a. Eigenvalues of the Cooperon matrix. To solve the equation (4.5) we first consider the following eigenvalue problem:[37]

$$\lambda_i \Psi_{ab}^{(i)} = \sum_{a'b'} \mathcal{M}_{aa',bb'}(0,0)\Psi_{a'b'}^{(i)}, \tag{4.8}$$

where the components of the matrix $\hat{\mathcal{M}}$ are given by (4.6). The quick calculation (see Appendix A for details) shows that $\mathcal{M}_{aa',bb'}(0,0) = \mathcal{M}_{aa'}\delta_{ab}\delta_{a'b'}$ with

$$\hat{\mathcal{M}} = \begin{pmatrix} \frac{\tau_\Gamma}{\tau_{\Gamma 0}} & \frac{\tau_X}{\tau_{\Gamma X}} & \frac{\tau_Y}{\tau_{\Gamma Y}} \\ \frac{\tau_\Gamma}{\tau_{X\Gamma}} & \frac{\tau_X}{\tau_{X0}} & \frac{\tau_Y}{\tau_{XY}} \\ \frac{\tau_\Gamma}{\tau_{Y\Gamma}} & \frac{\tau_X}{\tau_{YX}} & \frac{\tau_Y}{\tau_{Y0}} \end{pmatrix}. \tag{4.9}$$

The general expressions for the eigenvalues and the eigenvectors of this matrix are listed in Appendix B.

Next, we express the components of the Cooperon (4.8) in terms of the eigenvectors (4.8):

$$C_{00}^{ab,cd}(\omega,\mathbf{q}) = \sum_{ij} \mathcal{A}_{ij}(\omega,\mathbf{q}) \Psi_{ab}^{(i)} \Psi_{cd}^{(j)}, \tag{4.10}$$

Using this equation together with the normalization condition (B5), we can re-write the equation for the components of the Cooperon matrix (4.5) as follows:

$$\sum_k \left[(1-\lambda_i)\delta_{ik} + \mathcal{W}_{ik}(\omega,\mathbf{q})\right] \mathcal{A}_{kj}(\omega,\mathbf{q}) = \mathcal{V}_{ij}, \tag{4.11}$$

where the matrix elements $\mathcal{W}_{ik}(\omega,\mathbf{q})$ are given by

$$\mathcal{W}_{ik}(\omega,\mathbf{q}) = \\ = \sum_{ab,a'b'} [\mathcal{M}_{aa',bb'}(0,0) - \mathcal{M}_{aa',bb'}(\omega,\mathbf{q})]\Psi^{(i)}_{a'b'}\Psi^{(k)}_{ab} \tag{4.12}$$

and they are obviously vanishing for $\mathbf{q}\to 0$ and $\omega\to 0$. The matrix elements $\mathcal{V}_{ij}$ are obtained from expanding the first two terms in the right hand side of the Eq. (4.5) in terms of the eigenvectors $\Psi^{(i)}_{ab}$:

$$\Lambda_0\delta_{ac}\delta_{bd} + \Lambda_x[\hat{U}_x]_{ac}[\hat{U}_x]_{bd} = \sum_{ij}\mathcal{V}_{ij}\Psi^{(i)}_{ab}\Psi^{(j)}_{cd}. \tag{4.13}$$

It is straightforward to compute the coefficients $\mathcal{A}_{ij}(\omega,\mathbf{q})$ by solving the system of linear equations (4.11). For example, the coefficients $\mathcal{A}_{0j}(\omega,\mathbf{q})$, which contribute to the gapless Cooperon mode can be found by using the fact that the matrix elements $\mathcal{W}_{ik}(\omega,\mathbf{q})$ are small for small ω and $\mathbf{q}$. It follows

$$\mathcal{A}_{0j}(\omega,\mathbf{q}) \approx \frac{\mathcal{V}_{0j}}{\mathcal{W}_{00}(\omega,\mathbf{q})}. \tag{4.14}$$

For our subsequent analysis of the quantum correction to conductivity we will also need the remaining two contributions to the Cooperon. After some algebra we find that the resulting expression for the diagonal components of the Cooperon (4.7,4.10) can be written as follows:

$$C^a_{00}(\omega,\mathbf{q}) = \frac{\tau_t\Lambda_0}{\tau_a^2}\sum_{i=0}^{2}\frac{w_{ia}}{Dq^2 - i\omega + \Gamma_{ia}}, \tag{4.15}$$

where

$$\frac{1}{\tau_t} = \sum_a \frac{1}{\tau_a} \tag{4.16}$$

and the gaps in the denominator are

$$\Gamma_{0a} = 0, \quad \Gamma_{1a} = \tau_a^{-1}\gamma_+, \quad \Gamma_{2a} = \tau_a^{-1}\gamma_- \tag{4.17}$$

where $\gamma_\pm$ are expressed in terms of relaxation times (see Appendix B) and w_{ia} are dimensionless parameters determined by the combination of the intra- and interband scattering rates. In the expression above we introduced the diffusion coefficient for the singlet long-range mode entering into the expression for α, Eq. (1.3):

$$D = \sum_a\left[\frac{\tau_t}{\tau_{a0}}D_a + \sum_{b\neq a}\frac{\tau_t}{\tau_{ab}}D_b\right] \tag{4.18}$$

For the special case when $\tau_{\Gamma X} = \tau_{\Gamma Y}$ for the diffusion coefficient we find $D = (D_\Gamma\tau_X + 2D_X\tau_\Gamma)/(2\tau_\Gamma+\tau_X)$. Lastly, for reader's convenience, on Fig. 5 we plot the dependence of the coefficients $w_{1\Gamma}$ and $w_{2\Gamma}$ and the eigenvalues λ_i as the function of the ratio $\tau_\Gamma/\tau_{\Gamma 0}$ for the specific choice of the scattering times such that $\tau_a/\tau_{ba} = \tau_b/\tau_{ab}$.

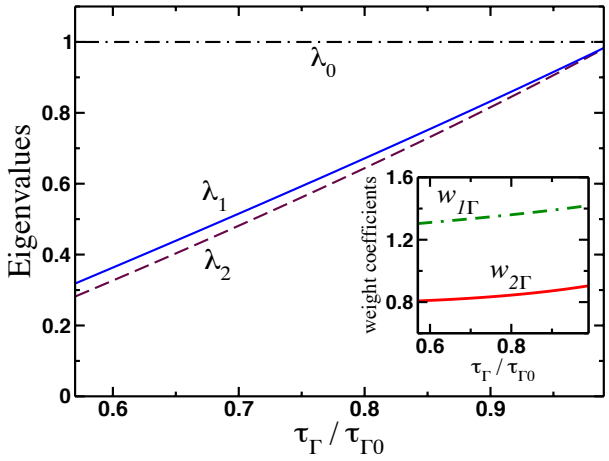

FIG. 5: (Color online) Plot of the eigenvalues λ_i $(i = 0, 1, 2)$ and the weight coefficients which appear in Eq. (4.15) as a function of $\tau_\Gamma/\tau_{\Gamma 0}$. Here without loss of generality we consider a special case when the following relation between the scattering times holds: $\frac{\tau_a}{\tau_{ba}} = \frac{\tau_b}{\tau_{ab}}$ $(a \neq b)$

Thus, we find that pseudospin symmetry breaking (band mixing) perturbations produce the relaxation in the spin-singlet components of the Cooperon except for the single mode, which is protected by the time-reversal symmetry.[35] The trajectories in Fig. 4(b) giving rise to the gapless Cooperon mode correspond to each ballistic segment the blue and red lines (moving in opposite directions shown by arrows) reside in the same electron band in the BZ and combine to form a spin-singlet. This is the pair of trajectories the interference between which is protected by time reversal, since time reversal maps each band on itself. Note that this is in contrast to the case of graphene where the time-reversal symmetry maps the two different bands on each other and therefore the band-singlet Cooperon mode is protected by time reversal symmetry[35]. In the following Section we evaluate the quantum correction to conductivity appearing due to the presence of this single long-range diffusion mode focusing specifically on the value of the pre-factor α appearing in the HLN formula (1.1).

B. WAL correction to conductivity

We again disregard the correction to conductivity arising from the triplet components as they are suppressed by the intraband scattering with the largest gap scale in our model. Moreover, we can omit gapped singlet modes due to the interband scattering keeping only the gapless mode identified in the previous section. This gapless mode is protected from dephasing due to the disorder scattering, but is still suppressed on length scales $l_\phi = \sqrt{D\tau_\phi}$ due to the inelastic electron scattering characterized by de-

coherence time τ_ϕ. We have, see Appendix B for details:

$$\delta\sigma \approx \sum_{a=\Gamma,X,Y} \left(2 - \frac{\tau_a}{\tau_{a0}}\right) e^2 \nu_a v_a^2 \tau_a^3 \times \\ \times \int C_{00}^a(\omega, \mathbf{q}) \frac{d\mathbf{q}}{(2\pi)^2}. \tag{4.19}$$

Carrying out the momentum integral, we find

$$\delta\sigma(0) = \frac{e^2}{2\pi^2} \left[\sum_a \frac{D_a \tau_t}{2D\tau_{a0}} \left(2 - \frac{\tau_a}{\tau_{a0}}\right)\right] \\ \times \sum_{i=0}^{2} w_{ia} \log\left(\frac{\tau_t^{-1}}{\max\{\tau_\phi^{-1}, \Gamma_{ia}\}}\right), \tag{4.20}$$

where τ_ϕ is the phase coherence time and we assumed $\tau_t^{-1} \gg \gamma_\pm \tau_a^{-1}$ $(i = 1, 2)$. Since $\delta\sigma(0) > 0$ the inteference correction leads to WAL.

Similarly to the calculation in Section III B in presence of an external magnetic field the summation over Landau levels yields the following expression for the magnetoconductivity $\delta\sigma(B)$:

$$\delta\sigma(B) = \frac{e^2}{2\pi^2} \left[\sum_a \frac{w_{0a} D_a \tau_t}{2D\tau_{a0}} \left(2 - \frac{\tau_a}{\tau_{a0}}\right)\right] \\ \times \left\{\Psi\left[\frac{1}{2} + \frac{B_0}{B}\left(\frac{l_\phi}{l_t}\right)^2\right] - \Psi\left[\frac{1}{2} + \frac{B_0}{B}\right]\right\}, \tag{4.21}$$

where we took into account the leading (gapless) contribution to the Cooperon, $l_\phi^2 = D\tau_\phi = 1/4eB_0$, $l_t^2 = D\tau_t$ and $\Psi(z)$ is the digamma function. The first digamma function in this expression can be replaced with $\log(B_0 l_\phi^2/B l_t^2)$ for $l_\phi/l_t \gg 1$ and we recover the structure of the HLN expression (1.1) for $\Delta\sigma(B) = \delta\sigma(B) - \delta\sigma(0)$.

For the moderately large magnetic fields, however, the remaining two modes will contribute to conductivity. Their contribution is formally given by the same expression as (4.21) where we have to replace τ_ϕ^{-1} with $\gamma_\pm \tau_a^{-1}$. It follows

$$\Delta\sigma_{\rm gap}(B) \approx \frac{e^2}{2\pi^2} \sum_{i=1}^{2} \frac{\alpha w_{ia}}{w_{0a}} \\ \times \left[\log\frac{B_i}{B} - \psi\left(\frac{1}{2} + \frac{B_i}{B}\right)\right] \tag{4.22}$$

with $4eB_i = (\gamma_\pm/D) \cdot \max\{\tau_\Gamma^{-1}, \tau_X^{-1}, \tau_Y^{-1}\}$, so that the total correction to conductivity becomes $\Delta\sigma_{\rm tot} = \Delta\sigma + \Delta\sigma_{\rm gap}$. Note, that unlike (4.21), the contribution from $\Delta\sigma_{\rm gap}$ is temperature independent.

In the limit of low magnetic field $B_i/B \gg 1$ the total quantum correction to conductivity $\Delta\sigma(B)$ simplifies to

$$\Delta\sigma(B \to 0) \approx -\frac{e^2}{24\pi^2\hbar} \sum_{i=0}^{2} \alpha_i \left(\frac{B}{B_i}\right)^2. \tag{4.23}$$

If we now compare this expression with (1.1) in the limit of small magnetic fields, we see that parameter α can be written as

$$\alpha = \sum_{i=0}^{2} \alpha_i \left(\frac{B_0}{B_i}\right)^2 \tag{4.24}$$

In the limit of infinite interband scattering times - $B_{1,2}$ become equal to B_0 and we recover the HLN formula with the pre-factor α given by Eq. (1.3). We also see that in the case when temperatures are not very low, $B_0 \sim B_i$ and even the gapped diffusion modes will nearly equally contribute to the localization correction.

To summarize, in the absence of the interband scattering, the eigenvalue problem (4.8) becomes degenerate, since in that case the second term on the right hand side of that equation vanishes, while the integral in the first term equals one. Therefore, in that case there will be three independent singlet long-range modes and in that case $\alpha = 3/2$. For finite albeit small interband scattering we find $\alpha \sim 1/2$ from Eq. (1.3). We note that the value of α is not universal due to asymmetry between of parameters for Γ and $X(Y)$ pockets. This non-universality on one hand is unexpected since in graphene, for example, one finds $\alpha = 1/2$ in the case of a single diffusion mode just like in the case of a two-dimensional electron gas with parabolic dispersion. We attribute the emergence of this non-universality to a combined effect three factors: only two out of three valleys are related by symmetry of the underlying lattice, difference in the diffusion coefficients on various Fermi pockets and the mismatch between the Fermi velocities, which enter into the conductivity diagrams, Fig. 7. Interestingly, non-universal value of α for the single diffusion mode resembles non-universal weak localization correction in a metal with partially polarized magnetic impurities when the rotational symmetry is broken.[38] It is important, however, to keep in mind that as temperature is decreased, one may expect a crossover behavior from $\alpha \sim 3/2$, when $\tau_\phi^{-1} \sim 4eDB_\gamma$ to $\alpha \sim 1/2$ for $\tau_\phi^{-1} \gg 4eDB_\gamma$, see Fig. 2.

C. WAL in correlated disorder

It will be instructive to consider the model for the mixture of correlated disorder, when the disorder potential at a given impurity site can scatter within the same valley as well as between different valleys, and compare the corresponding value of the weight factor in this case with the one found above (1.3).

For the correlated disorder mixture we consider the following model:

$$V(\vec{r}) = \sum_i u\hat{U}\delta(\vec{r} - \vec{R}_i), \quad \hat{U} = \hat{U}_0 + \zeta\hat{U}_x, \tag{4.25}$$

where $\hat{U}_0$, $\hat{U}_x$ are defined in Eq. (4.1) and coefficient $\zeta = u_x/u$. Now in addition to the two scattering times

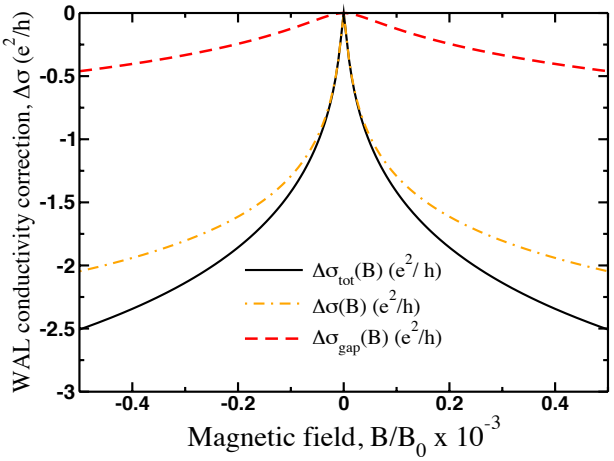

FIG. 6: (Color online) Plot of the total correction to conductivity $\Delta\sigma_{\rm tot}$) as a function of magnetic field for $\alpha = 0.45$. The values of the scattering rates and diffusion constants have been chosen as follows: $\tau_{\Gamma Y} = 1.2\tau_{\Gamma X}$, $\tau_{XY} = \tau_{\Gamma Y}$ and $D_X = D_Y = 0.95 D_\Gamma$.

τ_{a0} and τ_a defined previously (2.9,4.3) we also introduce the relaxation time due to disorder correlations:

$$\tau_{ax}^{-1} = \pi n_i \zeta u^2 \nu_a = \zeta \tau_{a0}^{-1}. \tag{4.26}$$

In turn, the self-energy matrix becomes off-diagonal in band indices due to disorder correlations:

$$\hat{\Sigma}_{ab}^{R,A}(\epsilon) \approx \mp \frac{i\hat{\sigma}_0}{2\tau_a} \mp \frac{i\hat{U}_x}{2\tau_{ax}}. \tag{4.27}$$

As a consequence of this, the matrix Green's function $\check{G}^{-1} = \check{G}_0^{-1} - \check{\Sigma}$ also becomes non-diagonal in band indices. However, in the computation of the Cooperon matrix within the required accuracy we can neglect the presence of the τ_{ax}^{-1} in the Green's functions. The reason is that in the calculation of the singlet components of the Cooperon, the matrix elements which are proportional to τ_{ax}^{-1} are of the order of $(p_F l)^{-1} \ll 1$ and therefore can be neglected.

The analysis of the Cooperon eigenvalues can now be done along the same lines as above. Specifically, the right hand side of the equation (4.8) will now acquire an extra term proportional to τ_{ax}^{-1}. Setting the eigenvalue $\lambda_0 = 1$ and solving for the eigenvectors within the required accuracy yields expressions similar to those found in Appendix B.

Finite τ_{ax} scattering time introduces off-diagonal in valley indices components of the Cooperon matrix, which give non-zero contribution to conductivity. However, the contribution of these off-diagonal terms is sub-leading in power of τ_a/τ_{ax} to the diagonal ones. If the off-diagonal Cooperon elements are neglected, the resulting expression for the coefficient α in the HLN formula reads

$$\alpha_x = \sum_a \frac{\widetilde{D}_a}{2\widetilde{D}} \left(2 - \frac{\tau_a}{\tau_{a0}}\right) \frac{\tilde{\tau}_t}{\tau_{a0}}, \tag{4.28}$$

where $\widetilde{D}_a = v_a^2 \tilde{\tau}_a$ and $\widetilde{D}$ is found by the same expression as in (4.18) by replacing $\tau_{t,a}$ with $\tilde{\tau}_{t,a}$ and $\tilde{\tau}_t^{-1} = \tilde{\tau}_\Gamma^{-1} + \tilde{\tau}_X^{-1} + \tilde{\tau}_Y^{-1}$. As we expected, the finite τ_{ax} further reduce the weak-antilocalization effect.

V. DISCUSSION AND CONCLUSIONS

Perhaps one of the main challenges in identifying the nature of the conducting surface states, such as the dispersion and helicity, in topological Kondo insulator such as SmB_6 lies in establishing to what extent the Dirac surface states remain well defined despite the fact that (a) hybridization between the conduction d- and f-orbitals is significantly reduced on the surface[39] and (b) the band bending effects due to disorder scattering on the surface, which leads to an appearance of the states inside the hybridization gap.[33] For example, recent ARPES measurements (see Ref. 40 and references therein) and low-frequency, radio-frequency and microwave conductivity[41] seem to be in support of the picture in which conventional Rashba-split bands dominate the low-temperature transport properties on the surface of SmB_6. On the other hand, recent radiation spectroscopy measurements and magneto-thermoelectric transport results and well as spin-resolved ARPES[21] support the picture of the topologically protected surface states. Interestingly, the Nernst effect data on the (011) plane reports the effective mass for the carries of the order of 100 of bare electron mass in agreement with existing theoretical estimates.[32,33]

Observation of the weak anti-localization correction to conductivity in topological insulators generally serves as an indication of the strong-spin orbit coupling and, therefore, is used to confirm the helicity of the conducting surface states. In topological Kondo insulators, however, the analysis of the experimental data is complicated by the possibility of the conventional polar bands which will be split by the Bychkov-Rashba spin-orbit coupling λ_{SO}. When disorder does not induce scattering between the Dirac and parabolic bands, one may expect a weak-antilocalization correction to conductivity provided the spin-orbit coupling is strong enough.[37,42]. Furthermore, the correction appears to be non-universal and is proportional to $(\lambda_{SO} p_F \tau_{\rm tr})^{-2}$ where $\tau_{\rm tr}$ is a transport time.[42] Clearly, whether the magnitude of this correction is of the same order as the one we find for Dirac electrons depends on the magnitude of the λ_{SO}: at strong Bychkov-Rashba splitting of the parabolic bands their contribution to conductivity quantum correction may be strongly suppressed by this additional factor. Lastly, for the scattering which mixes the Dirac bands with the parabolic bands, one single diffusion mode is expected to be present leading to $\alpha \sim 1/2$ for a given surface.

Another correction to our results above may appear due to the presence of magnetic scattering on the surface, which may change the picture of weak localization corrections presented above. In fact, based on the mag-

netoresistance data[31], it has been recently argued that unscreened f-electrons give rise to ferromagnetic state on the surface of SmB_6. One expects therefore, that the spin-flip scattering on the surface will gap out all Dirac bands completely suppressing transport. Even in the case when only one Dirac pocket is not gapped, the quantum interference correction to conductivity will be strongly suppressed. In addition, as it has been shown recently, the opening of the gap in the Dirac bands may actually change the sign in the quantum correction to conductivity from weak-antilocalization to weak localization.[25] Perhaps the fact that this crossover has not been observed[31] suggests that at least one of the Dirac bands remains ungapped.

In this paper, we have considered the quantum correction to conductivity in the model with three Dirac bands with intraband and interband disorder. We find that for the case of the interband disorder there is only one singlet long-range mode leading to the quantum correction to conductivity. The resulting expression for the weight factor shows that depending on the ratio between the diffusion coefficients and interband scattering times, one may expect the smooth crossover from $\alpha \sim 3/2$ to $\alpha \sim 1/2$. In contrast with the single band case when $\alpha = 1/2$, the presence of the interband scattering reduces the value of α so that it becomes non-universal. In fact, the interband scattering itself may be asymmetric, due to the large Fermi line missmatch between Γ and X, Y bands the scattering between them could be suppressed. In this case, independent contribution of the Γ in addition to the mixed X and Y components would result in $\alpha \approx 1$ which may explain the value observed in Ref. 30. Our results are generally in agreement with recent low-temperature transport experiments[30,31] on SmB_6.

Acknowledgments

This work was financially supported by KSU and MPI-PKS (M.D.), DARPA and Simons Foundation (V.G.), NSF Grant No. DMR-0955500 (M.V.) We thank Igor Aleiner, Leonid Glazman, Alex Levchenko and Jing Xia for useful discussions.

Appendix A: Components of the matrix $\hat{M}$

In this Section we provide an explicit derivation for the elements of the matrix $\hat{M}$ which enters into the equation for the Cooperon (3.2). This matrix is defined as follows

$$M^{ab}_{S_1S}(\omega,\mathbf{q}) = \frac{1}{2}\int \frac{d^2\mathbf{p}}{4\pi^2}\mathrm{Tr}\left\{[\hat{G}^R_a(\epsilon+\omega,\mathbf{p})]^T(\sigma_y\sigma_{S_1})[\hat{G}^A_b(\epsilon,\mathbf{q}-\mathbf{p})](\sigma_S\sigma_y)\right\} \tag{A1}$$

First, we compute the diagonal components in pseudospin space:

$$\begin{aligned}
M^{ab}_{00}(\omega,\mathbf{q}) &= \int \frac{d^2\mathbf{p}}{4\pi^2}\left\{\frac{(\epsilon+\omega+i/2\tau_a)(\epsilon-i/2\tau_b)+v_av_bp^2-v_av_b\mathbf{pq}}{[(\epsilon+\omega+i/2\tau_a)^2-v_a^2p^2][(\epsilon-i/2\tau_b)^2-v_b^2(\mathbf{q}-\mathbf{p})^2]}\right\},\\
M^{ab}_{11}(\omega,\mathbf{q}) &= \int \frac{d^2\mathbf{p}}{4\pi^2}\left\{\frac{(\epsilon+\omega+i/2\tau_a)(\epsilon-i/2\tau_b)+v_av_b[p_y(q_y-p_y)-p_x(q_x-p_x)]}{[(\epsilon+\omega+i/2\tau_a)^2-v_a^2p^2][(\epsilon-i/2\tau_b)^2-v_b^2(\mathbf{q}-\mathbf{p})^2]}\right\},\\
M^{ab}_{22}(\omega,\mathbf{q}) &= \int \frac{d^2\mathbf{p}}{4\pi^2}\left\{\frac{(\epsilon+\omega+i/2\tau_a)(\epsilon-i/2\tau_b)+v_av_b[p_x(q_x-p_x)-p_y(q_y-p_y)]}{[(\epsilon+\omega+i/2\tau_a)^2-v_a^2p^2][(\epsilon-i/2\tau_b)^2-v_b^2(\mathbf{q}-\mathbf{p})^2]}\right\},\\
M^{ab}_{33}(\omega,\mathbf{q}) &= \int \frac{d^2\mathbf{p}}{4\pi^2}\left\{\frac{(\epsilon+\omega+i/2\tau_a)(\epsilon-i/2\tau_b)-v_av_bp^2+v_av_b\mathbf{pq}}{[(\epsilon+\omega+i/2\tau_a)^2-v_a^2p^2][(\epsilon-i/2\tau_b)^2-v_b^2(\mathbf{q}-\mathbf{p})^2]}\right\}.
\end{aligned} \tag{A2}$$

We calculate each of these integrals separately. In what follows I use the following approximation

$$\omega\tau_{a,b} \ll 1, \quad v_j|\mathbf{q}-\mathbf{p}| \approx v_jp\left(1-\frac{q\cos\phi}{p_{Fj}}+\frac{q^2\sin^2\phi}{2p_{Fj}^2}\right) \tag{A3}$$

Consider the following integral

$$I_{ab} = \int \frac{d^2\mathbf{p}}{4\pi^2}\left\{\frac{1}{[(\epsilon+\omega+i/2\tau_a)^2-v_a^2p^2][(\epsilon-i/2\tau_b)^2-v_b^2p^2]}\right\} \tag{A4}$$

and introduce the following variables $\xi = \mathrm{sign}(\epsilon)v_a p - \epsilon$, $r_{ab} = v_a/v_b$. We have

$$I_{ab} = \frac{1}{2\pi v_b^2}\int\limits_{-\epsilon}^{\mathrm{sign}(\epsilon)\infty} \frac{[\mathrm{sign}(\epsilon)\xi + |\epsilon|]\mathrm{sign}(\epsilon)d\xi}{[(\epsilon+\omega+i/2\tau_a)^2 - v_a^2p^2][r_{ab}^2(\epsilon - i/2\tau_b)^2 - v_a^2p^2]} \approx$$
$$\approx \frac{|\epsilon|}{2\pi v_b^2}\frac{1}{2\epsilon^2(1+r_{ab})}\int\limits_{-\infty}^{+\infty}\frac{d\xi}{(\omega + i/2\tau_a - \xi)[(r_{ab}-1)\epsilon - i/2\tau_b - \xi]} \approx \tag{A5}$$
$$\approx \frac{2\pi\nu_b\tau_{ab}}{1 - 2i\omega\tau_{ab} - 2i(1-r_{ab})\epsilon\tau_{ab}}, \quad \tau_{ab}^{-1} = \tau_a^{-1} + \tau_b^{-1}.$$

Clearly, from this expression it follows that all off-diagonal elements of the Cooperon matrix will remain finite in zero momentum and frequency limit. Thus we need to analyze (A2) for $a = b$ only. We have

$$M_{00}^{aa} \approx 1 + i\omega\tau_a - \frac{v_a^2q^2\tau_a^2}{2}, \quad M_{33}^{aa} \approx -\frac{\omega + \frac{i}{\tau_a}}{2v_a p_{Fa}} \ll 1,$$
$$M_{11}^{aa} \approx \frac{1}{2}\left[1 + i\omega\tau_a - \frac{v_a^2q^2\tau_a^2}{2} - \frac{v_a^2q^2\tau_a^2\cos(2\varphi_q)}{4}\right], \quad M_{22}^{aa} \approx \frac{1}{2}\left[1 + i\omega\tau_a - \frac{v_a^2q^2\tau_a^2}{2} + \frac{v_a^2q^2\tau_a^2\cos(2\varphi_q)}{4}\right], \tag{A6}$$

where we used

$$\pi\nu_a\tau_a\Lambda = 1. \tag{A7}$$

Next, we consider the off-diagonal components is pseudospin space. We have:

$$M_{01}^{ab}(\omega,\mathbf{q}) = \int\frac{d^2\mathbf{p}}{4\pi^2}\left\{\frac{(\epsilon+\omega+i/2\tau_a)(q_x - p_x) + (\epsilon - i/2\tau_b)p_x}{[(\epsilon+\omega+i/2\tau_a)^2 - v_a^2p^2][(\epsilon - i/2\tau_b)^2 - v_b^2(\mathbf{q}-\mathbf{p})^2]}\right\},$$
$$M_{02}^{ab}(\omega,\mathbf{q}) = \int\frac{d^2\mathbf{p}}{4\pi^2}\left\{\frac{(\epsilon+\omega+i/2\tau_a)(q_y - p_y) + (\epsilon - i/2\tau_b)p_y}{[(\epsilon+\omega+i/2\tau_a)^2 - v_a^2p^2][(\epsilon - i/2\tau_b)^2 - v_b^2(\mathbf{q}-\mathbf{p})^2]}\right\}, \tag{A8}$$
$$M_{12}^{ab}(\omega,\mathbf{q}) = -\int\frac{d^2\mathbf{p}}{4\pi^2}\left\{\frac{(\epsilon+\omega+i/2\tau_a)p_y(q_x - p_x) + (\epsilon - i/2\tau_b)(q_y - p_y)p_x}{[(\epsilon+\omega+i/2\tau_a)^2 - v_a^2p^2][(\epsilon - i/2\tau_b)^2 - v_b^2(\mathbf{q}-\mathbf{p})^2]}\right\},$$

while the remaining components will give zero. Thus, collecting all the terms we obtain:

$$\hat{M} = \begin{bmatrix} \frac{v_a^2q^2\tau_a^2}{2} - i\omega\tau_a & -\frac{i}{2}v_aq\tau_a\cos\varphi_q & -\frac{i}{2}v_aq\tau_a\sin\varphi_q & 0 \\ -\frac{i}{2}v_aq\tau_a\cos\varphi_q & \frac{1}{2}\left(1 - i\omega\tau_a + \frac{v_a^2q^2\tau_a^2}{2} + \frac{v_a^2q^2\tau_a^2\cos(2\varphi_q)}{4}\right) & \frac{1}{8}v_a^2q^2\tau_a^2\sin(2\varphi_q) & 0 \\ -\frac{i}{2}v_aq\tau_a\sin\varphi_q & -\frac{1}{2}v_a^2q^2\tau_a^2\sin(2\varphi_q) & \frac{1}{2}\left(1 - i\omega\tau_a + \frac{v_a^2q^2\tau_a^2}{2} - \frac{v_a^2q^2\tau_a^2\cos(2\varphi_q)}{4}\right) & 0 \\ 0 & 0 & 0 & 1 \end{bmatrix}. \tag{A9}$$

This result shows that only single mode corresponding to the singlet component of the Cooperon matrix will remain gapless.

Appendix B: Eigenvalues and eigenvectors of the Cooperon matrix

The eigenvalues (4.8) of this matrix can be most compactly written in terms of the following parameters

$$r_{ab} = \frac{1}{2}\left(\frac{\tau_a}{\tau_{ab}}\frac{\tau_b}{\tau_{ba}} - t_at_b\right),\ t_a = \frac{1}{2}\left(\frac{\tau_a}{\tau_{a0}} - 1\right),\ \gamma_\pm = -\sum_a t_a \pm \sqrt{\left(\sum_a t_a\right)^2 + \sum_{a\neq b} r_{ab}} \tag{B1}$$

with $t_a = \frac{\tau_a}{2\tau_{a0}} - \frac{1}{2}$. Note that since the parameters $r_{ab} < 0$ and $t_a < 0$ the parameters $\gamma_\pm$ are positive. Then the expressions for the eigenvalues (4.8) are

$$\lambda_0 = 1, \quad \lambda_{1,2} = 1 - \gamma_\pm, \tag{B2}$$

Clearly, if we neglect the interband scattering, we find a threefold degenerate eigenvalue $\lambda = 1$. As we have discussed above this situation corresponds to the existence of three gapless modes. Inclusion of the interband scattering processes lifts the degeneracy leaving only one gapless mode. Below, we first show that $\gamma_\pm$ determine the gap for the diffusion modes and then compute the diffusion coefficient for the gapless mode.

b. Eigenvectors. From the analysis of the equation (4.11) it is clear that the diverging contribution to the Cooperon emerges for the eigenvalue $\lambda_0 = 1$ with the corresponding components of an eigenvector

$$\Psi^{(0)}_{ab} = N_0 \frac{\delta_{ab}}{\tau_a}, \tag{B3}$$

where $a = \Gamma, X, Y$ and proportionality coefficient N_0 is the normalization constant. Similarly, the eigenvector components for an eigenvalue $\lambda = 1 - \gamma_+$ are

$$\Psi^{(1)}_{ab} = \frac{N_1}{(1+\gamma_a)\tau_a}\delta_{ab} - \left(\sum_d \frac{N_0 N_1}{(1+\gamma_d)\tau_d^2}\right)\Psi^{(0)}_{ab}. \tag{B4}$$

Here N_1 is a normalization constant and $\gamma_a = \gamma_+ \tau_a^{-1}/(\tau_{\Gamma X}^{-1} + \tau_{\Gamma Y}^{-1} + \tau_{X\Gamma}^{-1})$. Similar expression can be obtained for the third eigenvector $\Psi^{(2)}_{ab}$. We note, that the eigenvectors $\Psi^{(i)}_{ab}$ satisfy the orthonormalization condition,

$$\sum_{a,b} \Psi^{(i)}_{ab}\Psi^{(j)}_{ab} = \delta_{ij}. \tag{B5}$$

Appendix C: Quantum corrections to conductivity

1. bare Hikami box

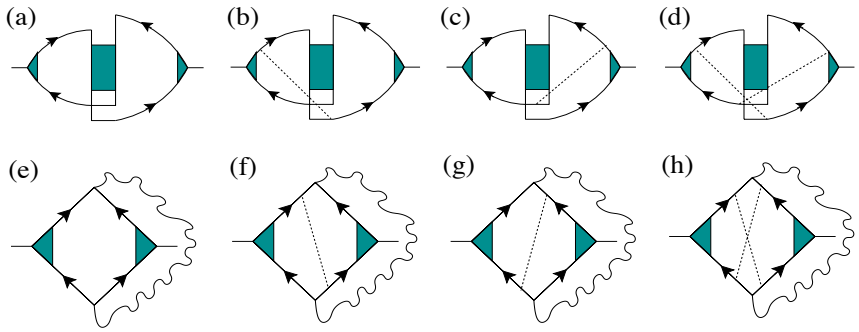

FIG. 7: (Color online) Panels (a)-(d): diagrams contributing to the weak localization correction to conductivity. Panels (e)-(h): the same contributions as (a)-(d), shown in the representation of Hikami boxes.

Contribution to conductivity from the bare Hikami box, Fig. 7(a,e), is:

$$\delta\sigma^{(1)}_{ij} = \frac{e^2}{2\pi}\int \frac{d\mathbf{k}d\mathbf{q}}{(2\pi)^4}\sum v_a v_b [\hat{G}^A_a(\mathbf{k},\epsilon)\sigma_i \hat{G}^R_a(\mathbf{k},\epsilon+\omega)]_{\alpha\beta}\Gamma^{ba,ba}_{\beta\delta\gamma\alpha}(\omega,\mathbf{q})[\hat{G}^R_b(\mathbf{q}-\mathbf{k},\epsilon+\omega)\sigma_j\hat{G}^A_b(\mathbf{q}-\mathbf{k},\epsilon)]_{\gamma\delta} \tag{C1}$$

To evaluate this correction we employ Eq. (2.19). Calculation of the trace over the pseudospin degrees of freedom is done by Mathematica. The resulting expression can be simplified by neglecting the dependence on external momentum $\mathbf{q}$ in the single particle correlators. In addition, as it follows from the calculation of the traces we can also neglect the frequency dependence in the denominators. We are interested in find the contribution from the most singular terms in the Cooperon. For the diagonal components of conductivity it follows

$$\begin{aligned}\delta\sigma^{(1)}_{ii} = \sum_{a=\Gamma,X,Y}\frac{e^2 v_a^2}{2\pi}\int\frac{d\mathbf{k}d\mathbf{q}}{(2\pi)^4}\sum_{S_1S_2}\frac{1}{2}C^a_{S_1S_2}(\mathbf{q})\mathrm{Tr}\Big\{\hat{G}^A_a(\mathbf{k},\epsilon)\sigma_i\hat{G}^R_a(\mathbf{k},\epsilon+\omega)\sigma_y^T\sigma^T_{S_1}\times\\ \times[\hat{G}^A_a(\mathbf{q}-\mathbf{k},\epsilon)]^T\sigma_i^T[\hat{G}^R_a(\mathbf{q}-\mathbf{k},\epsilon+\omega)]^T\sigma_y\sigma_{S_2}\Big\}\end{aligned} \tag{C2}$$

To calculate the trace we use the following relations:

$$[\hat{G}^{R,A}_a(\mathbf{k},\epsilon)]^T = \frac{\sigma_y[\epsilon_{R,A}\sigma_0 - v_a(k_x\sigma_x + k_y\sigma_y)]\sigma_y}{\epsilon^2_{R,A} - v_a^2k^2}, \quad \sigma_i^T = [2\delta_{i,0}-1]\sigma_y\sigma_i\sigma_y, \quad (i=0,x,y,z). \tag{C3}$$

Using these relations and neglecting the q dependence in the nominators of the $G^{A,R}$ for the trace we find

$$\begin{aligned}\frac{1}{2}\int\limits_0^{2\pi}\frac{d\phi}{2\pi}\mathrm{Tr}\left\{\hat{G}_a^A(\mathbf{k},\epsilon)\sigma_i\hat{G}_a^R(\mathbf{k},\epsilon+\omega)\sigma_y^T\sigma_{S_1}^T[\hat{G}_a^A(\mathbf{q}-\mathbf{k},\epsilon)]^T\sigma_i^T[\hat{G}_a^R(\mathbf{q}-\mathbf{k},\epsilon+\omega)]^T\sigma_y\sigma_{S2}\right\}\approx\\ \approx\delta_{S_1S_2}\epsilon^4\left\{4\delta_{S_1,0}-3\delta_{S_1,i}-\delta_{S_1,\bar{i}}\right\}\end{aligned}\tag{C4}$$

where on the last step I used $\omega\ll\epsilon$ and I have also assumed $v_ak\approx\epsilon$. Thus (C2) becomes

$$\delta\sigma_{ii}^{(1)}=\sum_{a=\Gamma,X,Y}\frac{e^2v_a^2}{2\pi}\int\frac{d\mathbf{q}}{(2\pi)^2}\left[4C_{00}^a(\mathbf{q})-3C_{ii}^a(\mathbf{q})-C_{\bar{i}\bar{i}}^a(\mathbf{q})\right]\int\frac{kdk}{2\pi}\frac{\epsilon^4}{[(\epsilon_R+\omega)^2-v_a^2k^2]^2[\epsilon_A^2-v_a^2k^2]^2}\tag{C5}$$

We deal with the momentum integral as follows:

$$\begin{aligned}\int\limits_0^\infty\frac{kdk}{2\pi}f(vk)=&\frac{1}{2\pi v^2}\int\limits_{-\epsilon}^{\mathrm{sign}(\epsilon)\infty}\{\mathrm{sign}(\epsilon)\varepsilon_k+|\epsilon|\}\,\mathrm{sign}(\epsilon)d\varepsilon_k f\left((\epsilon+\varepsilon_k)\mathrm{sign}(\epsilon)\right)\approx\\ \approx&\frac{|\epsilon|}{2\pi v^2}\int\limits_{-\infty}^{+\infty}f\left(\xi+|\epsilon|\right)d\xi=\nu\int\limits_{-\infty}^{+\infty}f\left(\xi+|\epsilon|\right)d\xi\end{aligned}\tag{C6}$$

Finally, the result is

$$\delta\sigma_{ii}^{(1)}=\sum_{a=\Gamma,X,Y}\frac{e^2\nu_av_a^2\tau_a^3}{8(1-i\omega\tau)^3}\int\frac{d\mathbf{q}}{(2\pi)^2}\left[4C_{00}^a(\mathbf{q})-3C_{ii}^a(\mathbf{q})-C_{\bar{i}\bar{i}}^a(\mathbf{q})\right].\tag{C7}$$

2. first disorder correction to the Hikami box

The expression for the second correction to conductivity, shown on Fig. 7(b,f), reads

$$\begin{aligned}\delta\sigma_{ii}^{(2)}=&\Lambda_0\sum_{a=\Gamma,X,Y}\frac{e^2v_a^2}{2\pi}\int\frac{d\mathbf{k}d\mathbf{p}d\mathbf{q}}{(2\pi)^6}\sum_{S_1S_2}\frac{1}{2}C_{S_1S_2}^a(\mathbf{q})\mathrm{Tr}\left\{\hat{G}_a^A(\mathbf{k},\epsilon)\sigma_i\hat{G}_a^R(\mathbf{k},\epsilon+\omega)\hat{U}\hat{G}_a^R(\mathbf{p},\epsilon+\omega)\sigma_y^T\sigma_{S_1}^T\times\right.\\ &\left.\times[\hat{G}_a^A(\mathbf{q}-\mathbf{p},\epsilon)]^T\sigma_i^T[\hat{G}_a^R(\mathbf{q}-\mathbf{p},\epsilon+\omega)]^T\hat{U}^T[\hat{G}_a^R(\mathbf{q}-\mathbf{k},\epsilon+\omega)]^T\sigma_y\sigma_{S_2}\right\}.\end{aligned}\tag{C8}$$

Here we took into account that only diagonal part of the disorder potential contributes to the conductivity correction, since correlation functions are diagonal in valley indices. Taking into account the expressions for the propagators and relations (C3) we obtain

$$\begin{aligned}\delta\sigma_{ii}^{(2)}=&\Lambda_0\sum_{a=\Gamma,X,Y}\frac{e^2v_a^2}{2\pi}\int\frac{d\mathbf{q}}{4\pi^2}\sum_{S_1S_2}\left(\delta_{S_1,0}-\frac{1}{2}\right)C_{S_1S_2}^a(\mathbf{q})\times\\ &\int\frac{pdp}{2\pi}\frac{1}{[(\epsilon_R+\omega+\frac{i}{2\tau})^2-v_a^2p^2]^2[(\epsilon-\frac{i}{2\tau})^2-v_a^2p^2]}\int\frac{kdk}{2\pi}\frac{1}{[(\epsilon_R+\omega+\frac{i}{2\tau})^2-v_a^2k^2]^2[(\epsilon-\frac{i}{2\tau})^2-v_a^2k^2]}\\ &\times\mathrm{Tr}\left\{[\epsilon_A\sigma_0+v_a(\mathbf{k}\cdot\vec{\sigma})]\sigma_i[(\epsilon_R+\omega)\sigma_0+v_a(\mathbf{k}\cdot\vec{\sigma})][(\epsilon_R+\omega)\sigma_0+v_a(\mathbf{p}\cdot\vec{\sigma})]\sigma_{S_1}\times\right.\\ &\left.\times[\epsilon_A\sigma_0+v_a(\mathbf{p}\cdot\vec{\sigma})]\sigma_i[(\epsilon_R+\omega)\sigma_0+v_a(\mathbf{p}\cdot\vec{\sigma})][(\epsilon_R+\omega)\sigma_0+v_a(\mathbf{k}\cdot\vec{\sigma})]\sigma_{S_2}\right\}.\end{aligned}\tag{C9}$$

Computation of the trace and subsequent integration over momenta in the limit $\omega=0$ yields

$$\delta\sigma_{ii}^{(2)}=-\sum_{a=\Gamma,X,Y}\frac{e^2\nu_av_a^2\tau_a^3}{8}\left(\frac{\tau_a}{\tau_{a0}}\right)\int\frac{d\mathbf{q}}{(2\pi)^2}\left[C_{00}^a(\mathbf{q})-C_{ii}^a(\mathbf{q})\right].\tag{C10}$$

Note, that an additional pre-factor appears since the relation time differs from the intra-pocket scattering time

3. second disorder correction to the Hikami box

The third correction, Fig. 7(c,g), is the same as the first correction (C10) to the Hikami box diagram:

$$\delta\sigma_{ii}^{(3)} = -\sum_{a=\Gamma,X,Y} \frac{e^2\nu_a v_a^2 \tau_a^3}{8}\left(\frac{\tau_a}{\tau_{a0}}\right)\int \frac{d\mathbf{q}}{(2\pi)^2}\left[C_{00}^a(\mathbf{q}) - C_{ii}^a(\mathbf{q})\right]. \tag{C11}$$

Finally, the fourth and the last correction to conductivity, Fig. 7 (d,g), is small in parameter $1/p_F l \ll 1$ and can be ignored. Adding up all three contributions to the conductivity we find expression (4.19) in the main text.

[1] M. Dzero, K. Sun, V. Galitski, and P. Coleman, Phys. Rev. Lett. **104**, 106408 (2010).
[2] T. Takimoto, Journal of Physical Society of Japan **80**, 123710 (2011).
[3] M. Dzero, K. Sun, P. Coleman, and V. Galitski, Phys. Rev. B **85**, 045130 (2012).
[4] X. Deng, K. Haule, and G. Kotliar, Phys. Rev. Lett. **111**, 176404 (2013).
[5] F. Lu, J. Zhao, H. Weng, Z. Fang, and X. Dai, Phys. Rev. Lett. **110**, 096401 (2013).
[6] H. Weng, J. Zhao, Z. Wang, Z. Fang, and X. Dai, Phys. Rev. Lett. **112**, 016403 (2014), URL http://link.aps.org/doi/10.1103/PhysRevLett.112.016403.
[7] M. Z. Hasan and C. L. Kane, Rev. Mod. Phys. **82**, 3045 (2010), URL http://link.aps.org/doi/10.1103/RevModPhys.82.3045.
[8] J. W. Allen, B. Batlogg, and P. Wachter, Phys. Rev. B **20**, 4807 (1979).
[9] J. C. Cooley, M. C. Aronson, Z. Fisk, and P. C. Canfield, Phys. Rev. Lett. **74**, 1629 (1995).
[10] P. Nyhus, S. L. Cooper, Z. Fisk, and J. Sarrao, Phys. Rev. B **55**, 12488 (1997).
[11] P. S. Riseborough, Advances in Physics **49**, 257 (2000).
[12] T. Caldwell, A. P. Reyes, W. G. Moulton, P. L. Kuhns, M. J. R. Hoch, P. Schlottmann, and Z. Fisk, Phys. Rev. B **75**, 075106 (2007).
[13] S. Wolgast, C. Kurdak, K. Sun, J. W. Allen, D.-J. Kim, and Z. Fisk, Phys. Rev. B **88**, 180405 (2013).
[14] D. J. Kim, S. Thomas, T. Grant, J. Botimer, Z. Fisk, and J. Xia, Sci. Rep. **3** (2013).
[15] X. Zhang, N. P. Butch, P. Syers, S. Ziemak, R. L. Greene, and J. Paglione, Phys. Rev. X **3**, 011011 (2013).
[16] G. Li et al. (2013), arXiv:1306.5221.
[17] M. C. Hatnean, M. R. Lees, D. M. Paul, and G. Balakrishnan, Sci. Rep. **3** (2013).
[18] D. J. Kim, J. Xia, and Z. Fisk, Nat Mater **13**, 466 (2014).
[19] P. P. Baruselli and M. Vojta, Phys. Rev. B **89**, 205105 (2014).
[20] W. A. Phelan, S. M. Koohpayeh, P. Cottingham, J. W. Freeland, J. C. Leiner, C. L. Broholm, and T. M. McQueen, Phys. Rev. X **4**, 031012 (2014).
[21] N. Xu, P. K. Biswas, J. H. Dil, R. S. Dhaka, G. Landolt, S. Muff, C. E. Matt, X. Shi, N. C. Plumb, M. Radović, et al., Nat Commun **5** (2014), URL http://dx.doi.org/10.1038/ncomms5566.
[22] N. Wakeham, Y. Q. Wang, Z. Fisk, F. Ronning, and J. D. Thompson, Phys. Rev. B **91**, 085107 (2015), URL http://link.aps.org/doi/10.1103/PhysRevB.91.085107.
[23] Y. Luo, H. Chen, J. Dai, Z.-a. Xu, and J. D. Thompson, Phys. Rev. B **91**, 075130 (2015), URL http://link.aps.org/doi/10.1103/PhysRevB.91.075130.
[24] S. Hikami, A. Larkin, and Y. Nagaoka, Progress in Theoretical Physics **63**, 707 (1980).
[25] H.-Z. Lu, J. Shi, and S.-Q. Shen, Phys. Rev. Lett. **107**, 076801 (2011), URL http://link.aps.org/doi/10.1103/PhysRevLett.107.076801.
[26] G. Tkachov and E. M. Hankiewicz, Phys. Rev. B **84**, 035444 (2011), URL http://link.aps.org/doi/10.1103/PhysRevB.84.035444.
[27] H.-Z. Lu and S.-Q. Shen, Phys. Rev. B **84**, 125138 (2011), URL http://link.aps.org/doi/10.1103/PhysRevB.84.125138.
[28] I. Garate and L. Glazman, Phys. Rev. B **86**, 035422 (2012), URL http://link.aps.org/doi/10.1103/PhysRevB.86.035422.
[29] X.-L. Qi and S.-C. Zhang, Rev. Mod. Phys. **83**, 1057 (2011), URL http://link.aps.org/doi/10.1103/RevModPhys.83.1057.
[30] S. Thomas, D. J. Kim, S. B. Chung, T. Grant, Z. Fisk, and J. Xia (2013), arXiv1307.4133.
[31] Y. Nakajima, P. S.Syers, X. Wang, R. Wang, and J. Paglione, *One-dimensional edge state transport in a topological kondo insulator* (2013), arXiv:1312.6132.
[32] V. Alexandrov, M. Dzero, and P. Coleman, Phys. Rev. Lett. **111**, 226403 (2013).
[33] B. Roy, J. D. Sau, M. Dzero, and V. Galitski, Phys. Rev. B **90**, 155314 (2014), URL http://link.aps.org/doi/10.1103/PhysRevB.90.155314.
[34] Z.-H. Zhu, A. Nicolaou, G. Levy, N. P. Butch, P. Syers, X. F. Wang, J. Paglione, G. A. Sawatzky, I. S. Elfimov, and A. Damascelli, Phys. Rev. Lett. **111**, 216402 (2013), URL http://link.aps.org/doi/10.1103/PhysRevLett.111.216402.
[35] E. McCann, K. Kechedzhi, V. I. Fal'ko, H. Suzuura, T. Ando, and B. L. Altshuler, Phys. Rev. Lett. **97**, 146805 (2006), URL http://link.aps.org/doi/10.1103/PhysRevLett.97.146805.
[36] D. Rainer and G. Bergmann, Phys. Rev. B **32**, 3522 (1985), URL http://link.aps.org/doi/10.1103/PhysRevB.32.3522.
[37] N. Averkiev, L. Golub, and G. Pikus, Journal of Experimental and Theoretical Physics **86**, 780 (1998), ISSN 1063-7761, URL http://dx.doi.org/10.1134/1.558539.
[38] M. G. Vavilov and L. I. Glazman, Phys. Rev. B **67**,

115310 (2003), URL http://link.aps.org/doi/10.1103/PhysRevB.67.115310.

[39] V. Alexandrov, P. Coleman, and O. Erten (2015), arxiv:1501.03031.

[40] P. Hlavenka et al., *Samarium hexaboride: a trivial surface conductor* (2015), arXiv:1502.01542.

[41] N. E. Sluchanko, V. V. Ġlushkov, B. P. Gorshunov, S. V. Demishev, M. V. Kondrin, A. A. Pronin, A. A. Volkov, A. K. Savchenko, G. Grüner, Y. Bruynseraede, et al., Phys. Rev. B **61**, 9906 (2000), URL http://link.aps.org/doi/10.1103/PhysRevB.61.9906.

[42] M. Skvortsov, Journal of Experimental and Theoretical Physics Letters **67**, 133 (1998), ISSN 0021-3640, URL http://dx.doi.org/10.1134/1.567636.